Supporting Information

Unveiling microscopic carrier loss mechanisms in 12% efficient $Cu_2ZnSnSe_4$ solar cells

Jianjun Li[a#]*, *Jialiang Huang*[a#], *Fajun Ma*[a#], *Heng Sun*[a], *Jialin Cong*[a], *Karen Privat*[b], *Yin Yao*[b], *Robert Lee Chin*[a], *Mingrui He*[a], *Kaiwen Sun*[a], *Hui Li*[c], *Yaohua Mai*[d], *Ziv Hameiri*[a], *Nicholas J. Ekins-Daukes*[a], *Richard D. Tilley*[b], *Thomas Unold*[e], *Martin A. Green*[a], *Xiaojing Hao*[a]*

[a] Australian Centre for Advanced Photovoltaics, School of Photovoltaic and Renewable Energy Engineering, University of New South Wales, Sydney, NSW 2052, Australia.

[b] Electron Microscope Unit, Mark Wainwright Analytical Centre, University of New South Wales, Sydney, NSW 2052, Australia.

[c] Beijing National Laboratory for Condensed Matter Physics, Institute of Physics, Chinese Academy of Sciences, Beijing 100190, China

[d] Institute of New Energy Technology, College of Information Science and Technology, Jinan University, Guangzhou 510632, China.

[e] Helmholtz-Zentrum für Materialien und Energie, Hahn-Meitner-Platz 1, 14109 Berlin, Germany

*Correspondence should be addressed to J.L. (jianjun.li@unsw.edu.au) or X.H. (xj.hao@unsw.edu.au)

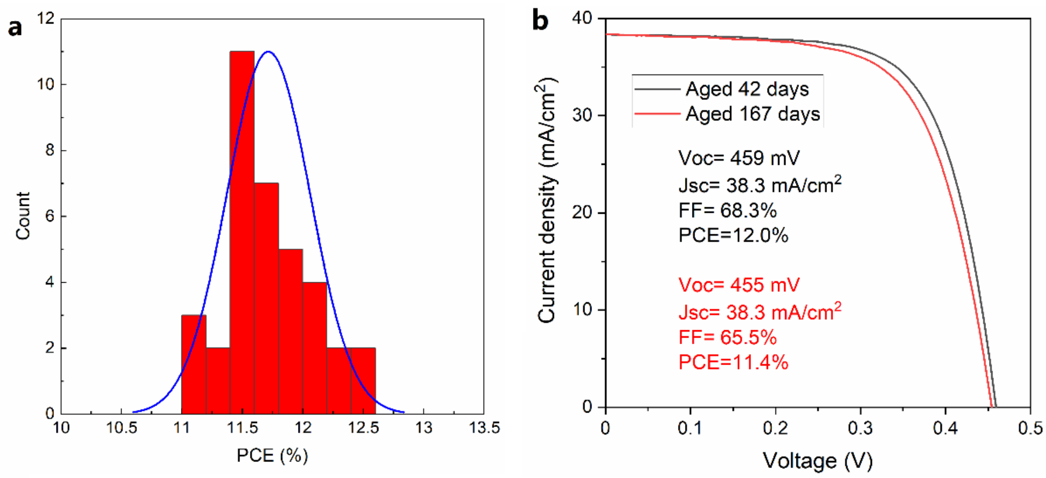

Figure S1. a Histogram of the power conversion efficiencies of the CZTSe solar cells using the same CZTSe absorbers fabricated in this work. 36 cells are included. **b** I-V curves of an un-capsulated CZTSe solar cell aged in a nitrigen box (30% to 40% humidity) for 42 days and 167 days respectively.Due to the pandemic lockdown, the first I-V measurement was performed 42 days after the completion of the device.

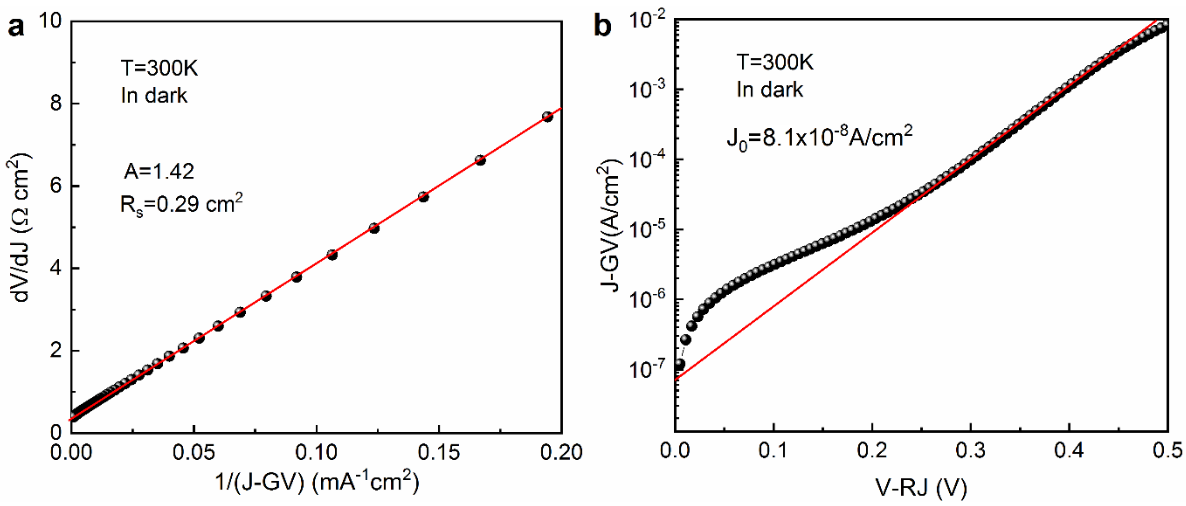

Figure S2. The fitting results of (**a**) Rs, A and (**b**) J_0 of the high efficiency CZTSe solar cell using the dark J-V curve at room temperature.

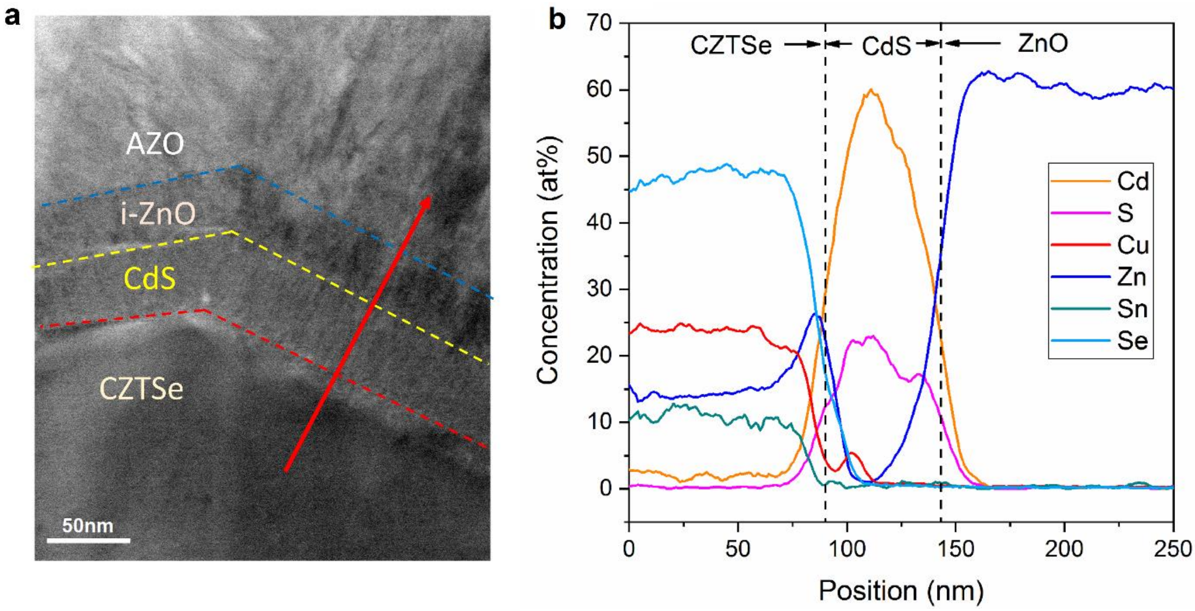

Figure S3 a TEM image of the CZTSe/CdS/ZnO heterointerfaces. **b** Element profile from the EDS line-scan at the region indicated by the red arrow in **a**.

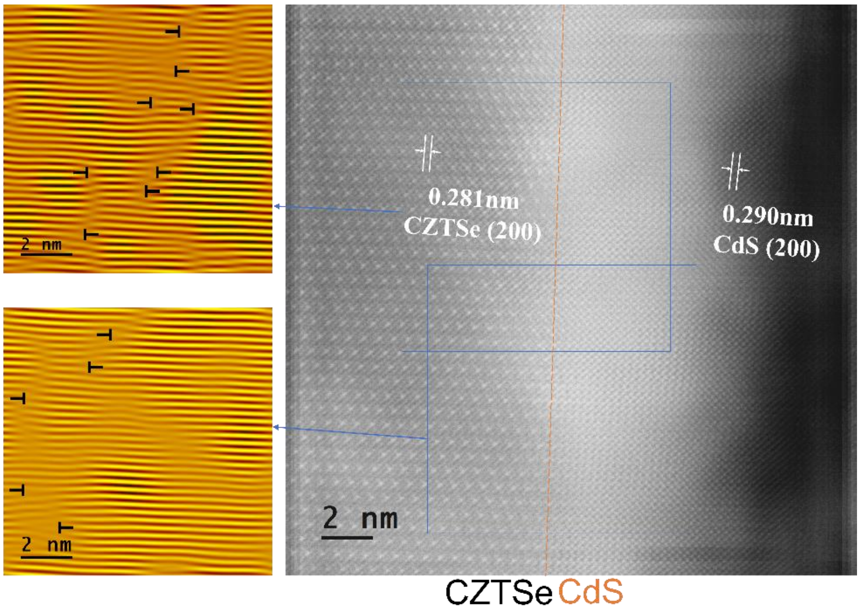

Figure S4. HRTEM image and the color-coded inverse fast Fourier transformation (FFT) images of the selected reflections revealing the dislocations (T marked) at the CZTSe/CdS heterointerface.

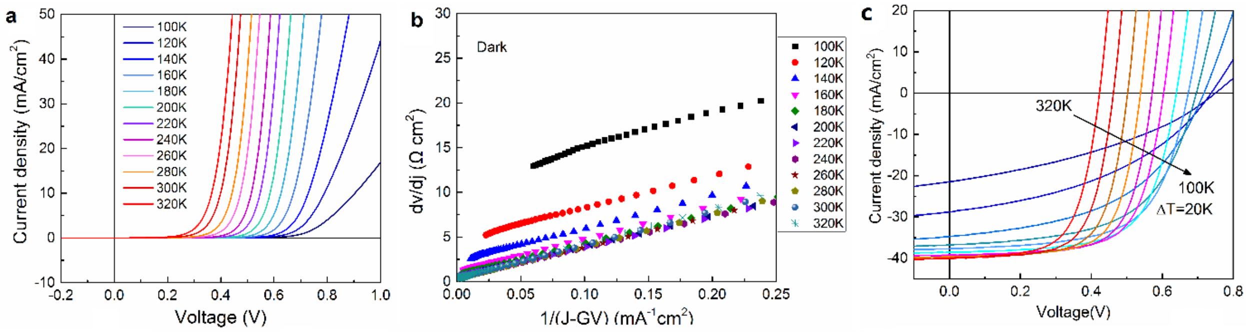

Figure S5. a Temperature dependent J-V curves in dark. **b** Fits of temperature dependent Rs and A using the J-V data. **c** Temperature dependent J-V curves under one sum illumination.

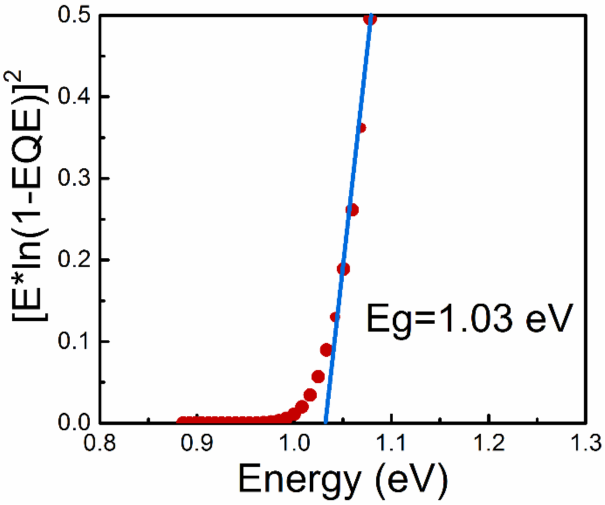

Figure S6. The fit of band gap derived from the EQE data.

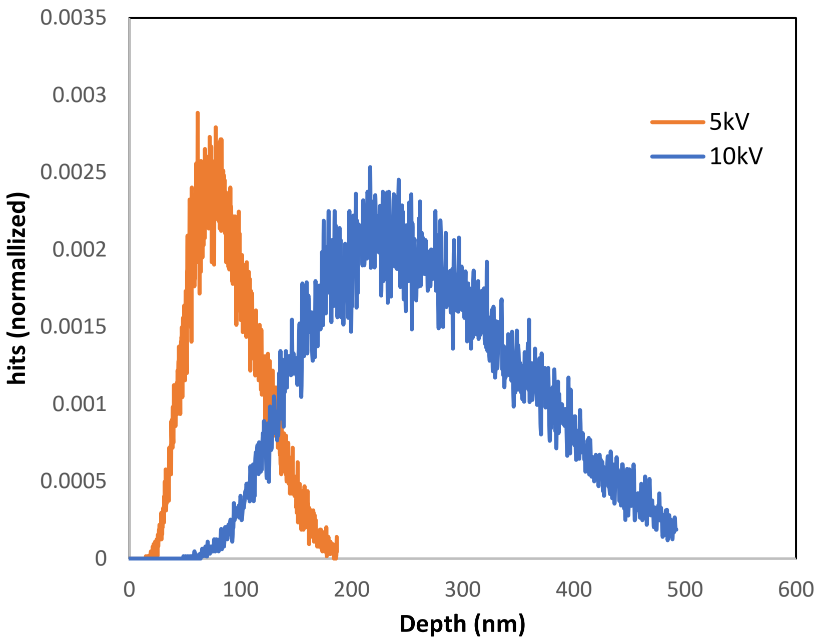

Figure S7. Simulated excitation depth of electron beam energy of 5keV and 10keV by Monte Carlo method using the CASINO software.

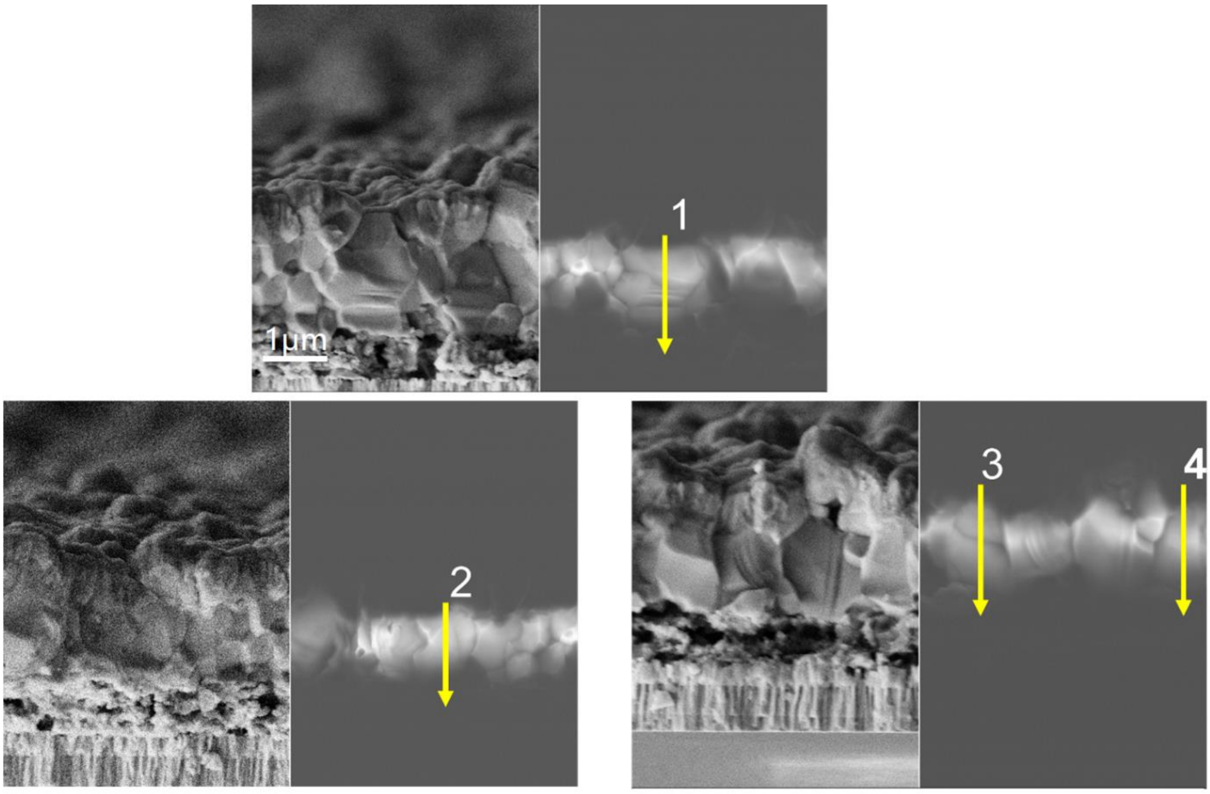

Figure S8. Cross-section SEM image (left) and EBIC image (right) of the cleaved CZTSe device at different regions. The yellow arrows indicates where EBIC line profile are taken.

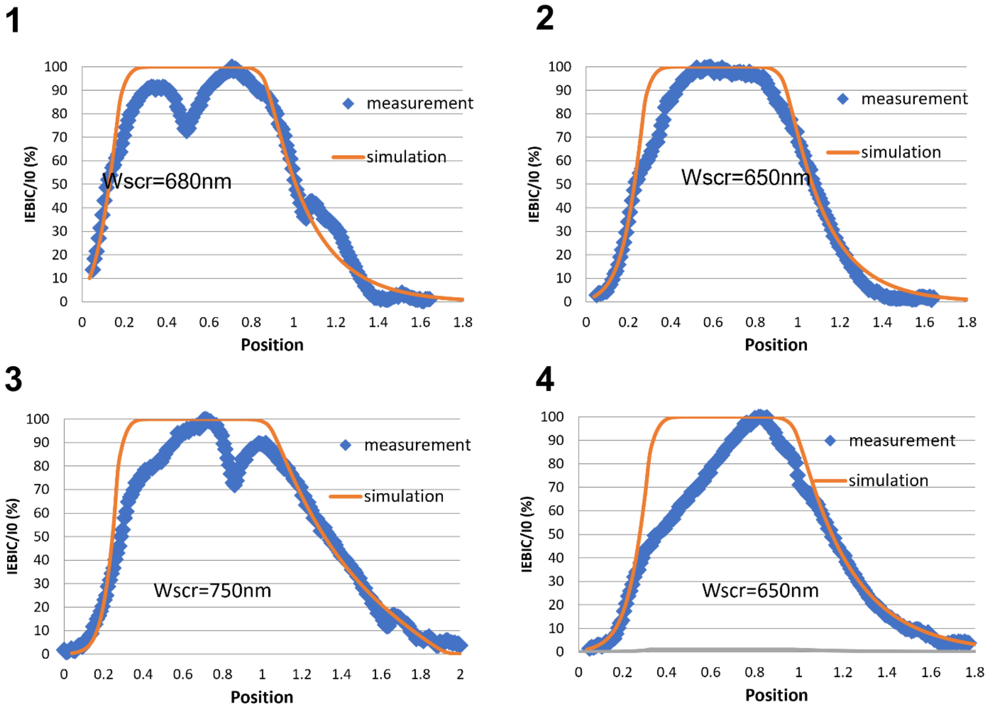

Figure S9. Extracted EBIC profiles along the corresponding yellow arrows in Figure S9. The space charge region width, Wscr is fitted using the analytical model described in Ref [1].

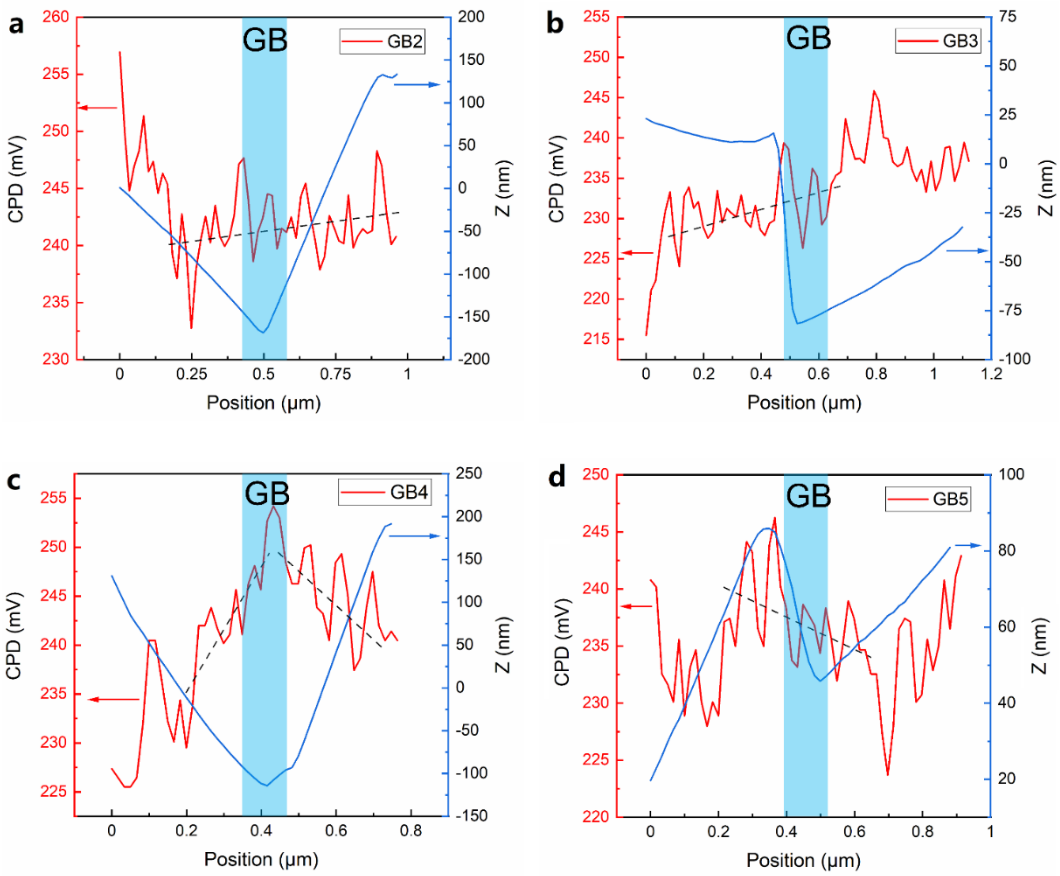

Figure S10. The CPD and topology profiles of GB2- GB5 indicated in **Figure 4 a** and **4b**. The dash lines are the visual guide of the average CPD distribution neat the GBs.

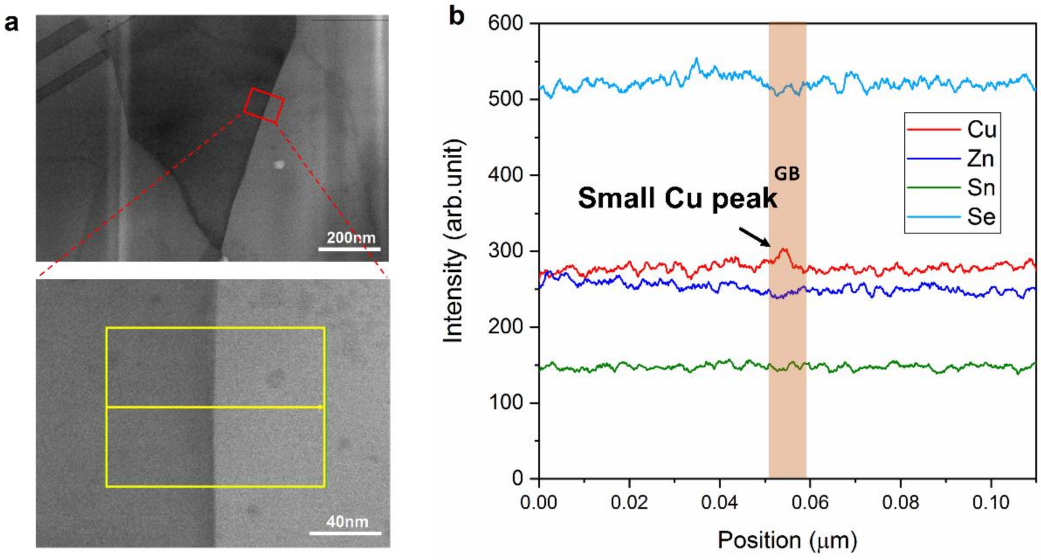

Figure S11. a TEM image of a GB where EDS line-scan in **b** was taken. The EDS line-scan shows a slight Cu peak at the GB.

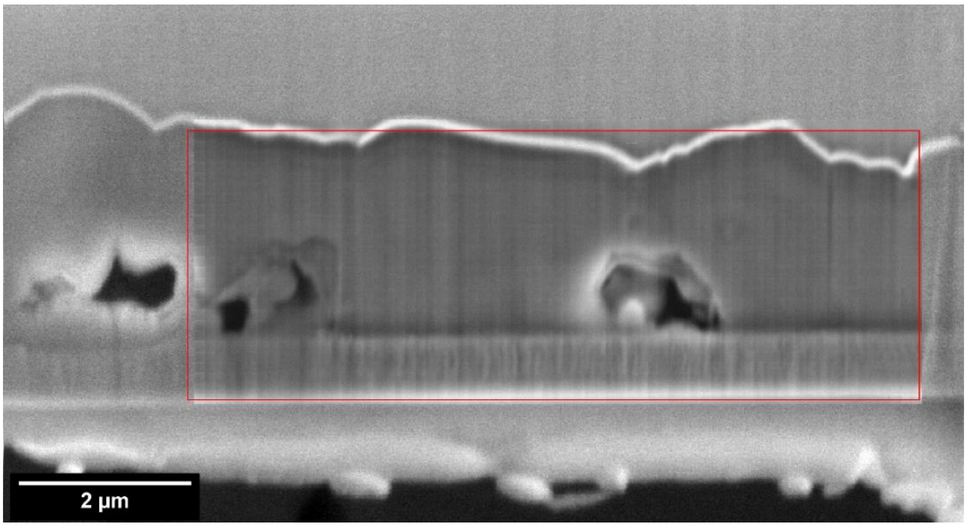

Figure S12. SEM image of the sample used for CL measurement.

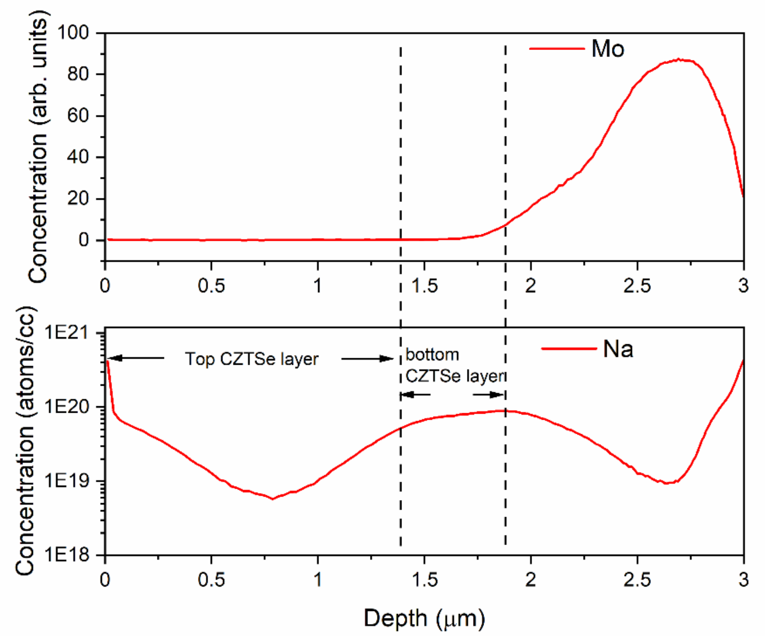

Figure S13. Na and Mo depth profile of the CZTSe absorber measured by SIMS. This data was aquired together with the SIMS data in Figure 1d.

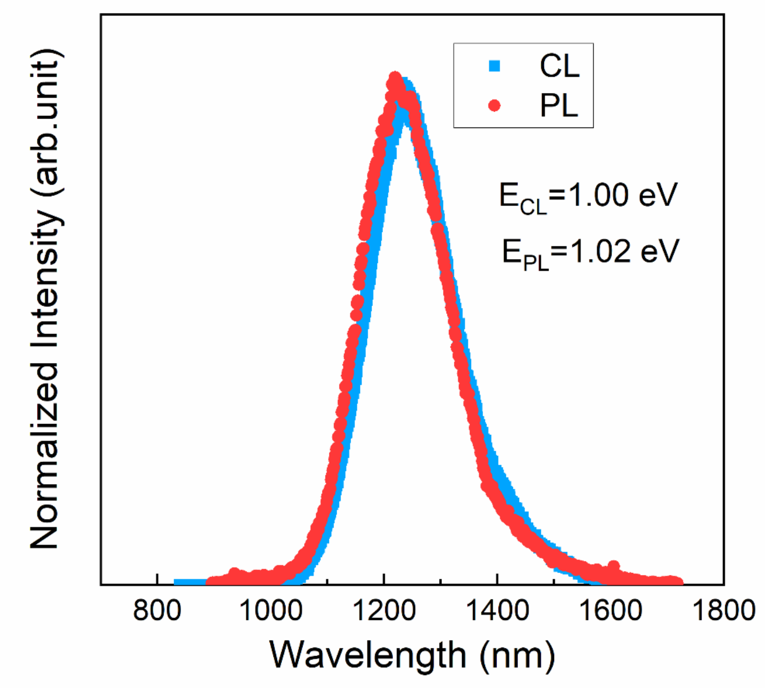

Figure S14. The cathodoluminescence and photoluminescence spectra of the CZTSe film.

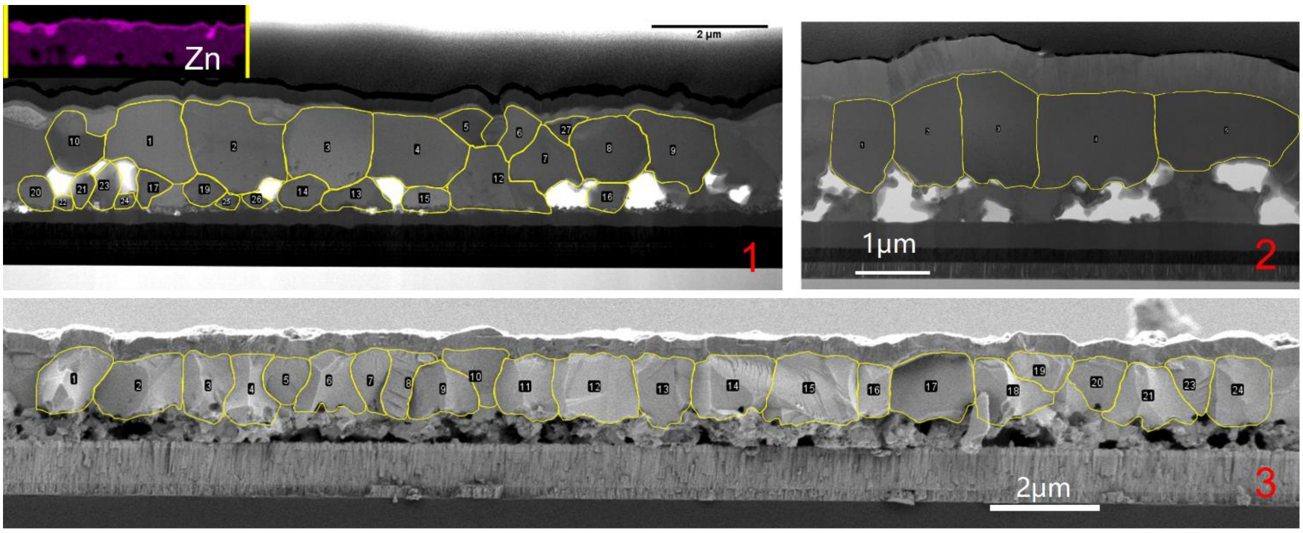

Figure S15. Cross-section TEM (**1** and **2**) and SEM(**3**) images of CZTSe solar cells. The yellow frames are manually plotted along the grain boundaries to define the grain size of each grain.

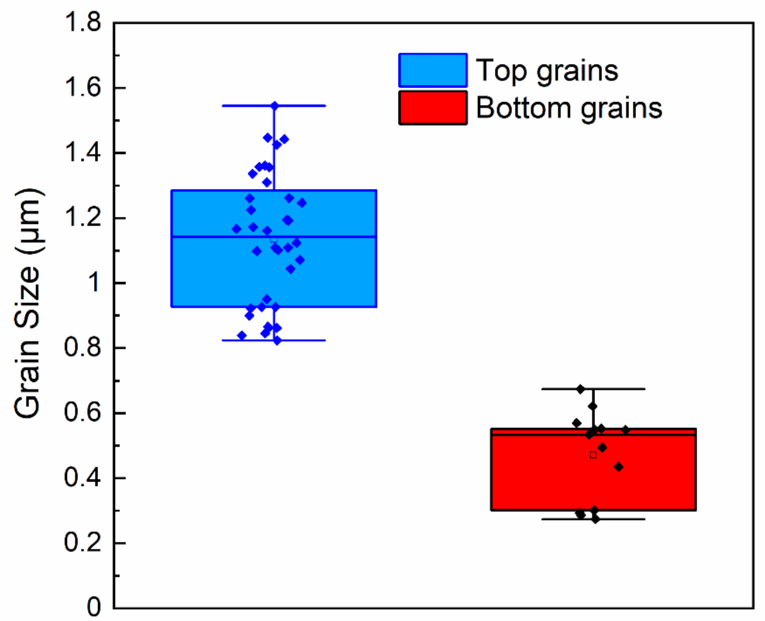

Figure S16. Statistic grain size extracted from cross-section TEM and SEM images in Figure S13. A grain size is approximately calculated as the square root of the area of the grain. The grains directly connect to buffer layer are regarded as the "top" grains while the others are regarded as "bottom" grains. The average size of "top" grains is 1.1 µm and the average size of "bottom" grains is 0.5 µm.

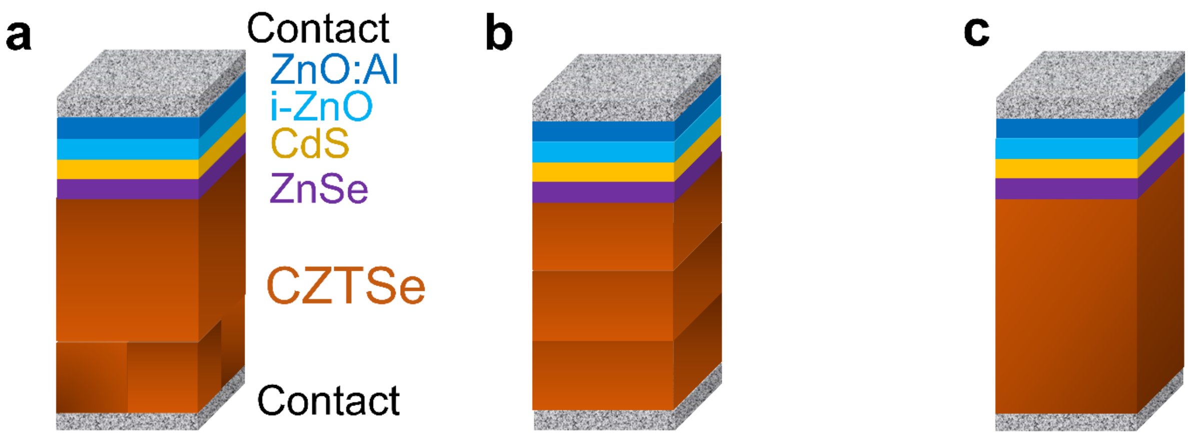

Figure S17. The schematic of the unit cells: (a) the reference cell with 1.1 µm top grains and 0.5 µm bottom grains; (b) the 0.5 µm grains cell; (c) the 3 µm grain cell. The thickness of CZTSe absorber is fixed at 1.5 to 1.6 µm.

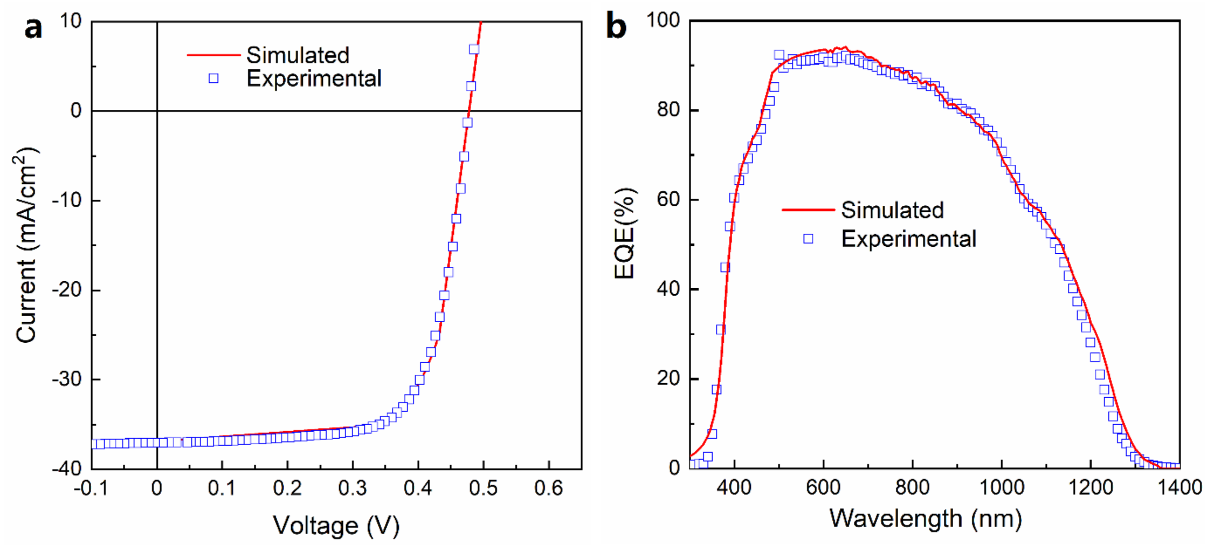

Figure S18. The simulated and experimental JV (a) and EQE (b) curves of CZTSe devices.

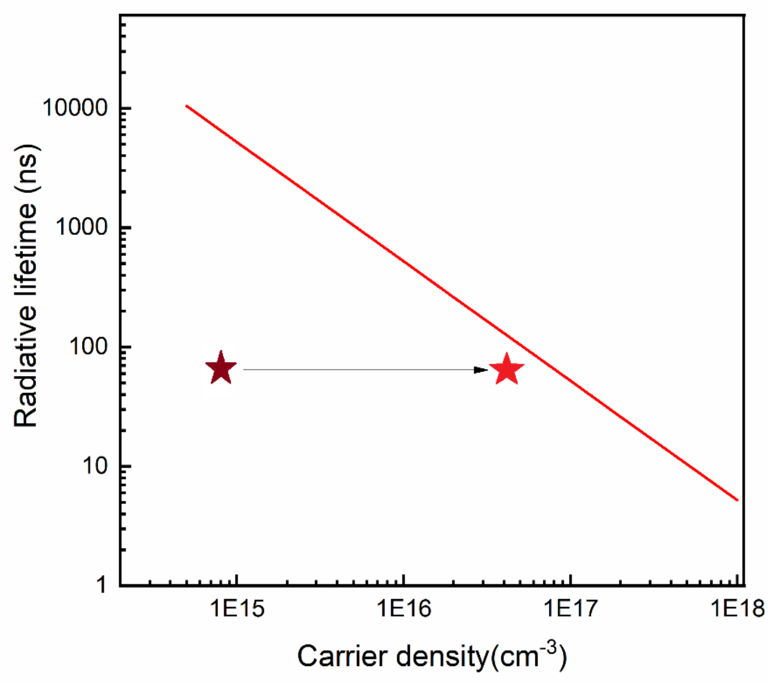

Figure S19. The radiative minority carrier lifetime vs. hole carrier density of CZTSe materials according to the radiative limit: $\tau_{rad} = 1/BN$, where τ_{rad} is the radiative recombination lifetime, B is the radiative recombination probability, and N is the carrier density. Here, B could be extracted using the equation defined by the electron and hole effective masses, dielectric constant, and bandgap: $B = 0.58 \times 10^{-12}\sqrt{\varepsilon}\left(\frac{1}{m_p+m_n}\right)^{1.5}\left(1+\frac{1}{m_p}+\frac{1}{m_n}\right) \times \left(\frac{300}{T}\right)^{1.5} E_g^2\ [cm^3 sec^{-1}]$.[1,2] Using $m_e^* = 0.08$ and $m_h^* = 0.21$,[3] B for CZTS is calculated to be 1.9×10^{-10} cm^3/sec.

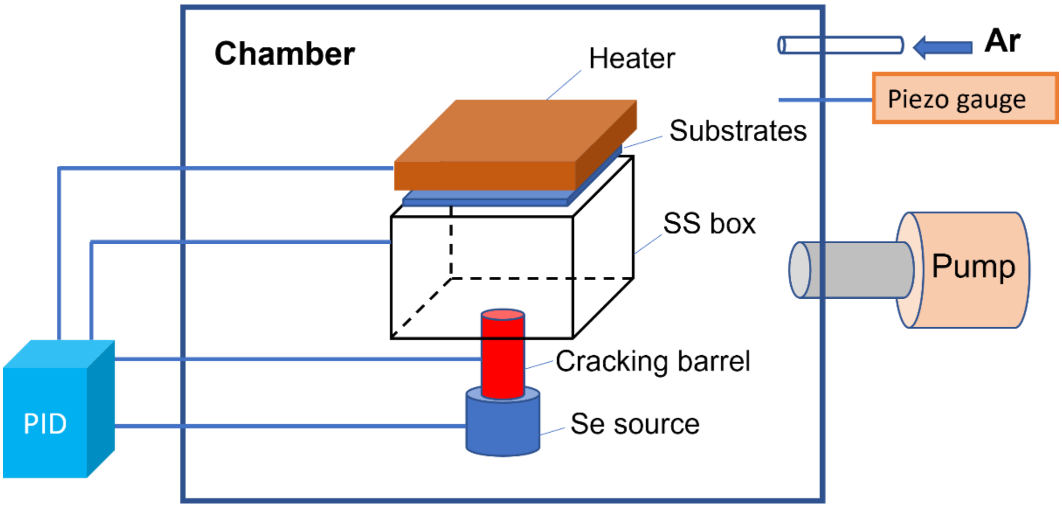

Figure S20. Schematic diagram of the custom-made Se furnace used for the selenization annealing. The piezo gauge is a piezoelectric gauge which works between 1-100kPa. The substrates are face-down placed, and the substrate heater is made of molybdenum wires. A thermo couple directly contacting with the back of substrate is used to monitor the substrate temperature. The temperature of the stainless-steel box is maintained at around 200°C during pre-alloying treatment while around 450°C during selenization. Details of Se atmosphere control can be find in Ref. 4.

Table S1: Key semiconductor parameters used for 3D simulations. The absorption of CZTSe was taken from Ref. 5.

Material	Parameters	Electron	Hole	Unit
CdS	Relative permittivity	10		
	Thickness	20		nm
	Electron affinity	4.2		eV
	Bandgap	2.4		eV
	Density of states	2.20E+18	1.80E+19	cm^{-3}
	Constant mobility	100	25	$cm^2V^{-1}s^{-1}$
	Doping	1.00E+17	NA	cm^{-3}
ZnSe	Relative permittivity	8.6		
	Thickness	5		nm
	Electron affinity	4.09		eV
	Bandgap	2.7		eV
	Density of states	1.61E+18	1.63E+19	cm^{-3}
	Constant mobility	400	110	$cm^2V^{-1}s^{-1}$
	Doping	1.00E+12	NA	cm^{-3}
CZTSe	Relative permittivity	8.6		
	Thickness	1600		nm
	Electron affinity	4.54		eV
	Bandgap	1.02		eV
	Density of states	5.66E+17	2.41E+18	cm^{-3}
	Constant mobility	20	10	$cm^2V^{-1}s^{-1}$
	Doping	NA	8.00E+14	cm^{-3}
	SRH lifetime	50	50	ns

Table S2. Simulated impact of intragrain minority carrier lifetime τ_{GI} on device performance, and $S_{GB,eff}$ 7000 cm s^{-1}.

τ_{GI} (ns)	1	5	10	50	100	500	1000
J_{sc} (mA/cm^2)	33.57	36.22	36.59	36.89	36.93	36.96	36.96
V_{oc} (mV)	431.61	463.98	470.44	477.88	479.04	480.02	480.15
η (%)	8.16	11.07	11.71	12.38	12.48	12.56	12.57
FF (%)	56.32	65.87	68.05	70.25	70.56	70.80	70.84

Table S3. Simulated impact of grain size on device performance, with intragrain lifetime 50 ns and $S_{GB,eff}$ 7000 cm s^{-1}.

Grain size	0.5 µm	1 µm	3 µm
J_{sc} **(mA/cm^2)**	36.15	36.87	37.31
V_{oc} **(mV)**	474.68	496.33	506.22
η **(%)**	11.10	12.13	13.54
FF **(%)**	64.70	66.28	71.68

References:

1. Yamaguchi, M.; Tampo, H.; Shibata, H.; Lee, K.-H.; Araki, K.; Kojima, N.; Ohshita, Y., Analysis for non-radiative recombination and resistance loss in chalcopyrite and kesterite solar cells. *Japanese Journal of Applied Physics* **2021,** *60* (SB).
2. Ahrenkiel, R. K.; Lundstrom, M. S., *Semiconductors and semimetals*. Academic Press: 1993.
3. Persson, C., Electronic and optical properties of Cu[sub 2]ZnSnS[sub 4] and Cu[sub 2]ZnSnSe[sub 4]. *Journal of Applied Physics* **2010,** *107* (5), 053710.
4. Li, J.; Wang, H.; Wu, L.; Chen, C.; Zhou, Z.; Liu, F.; Sun, Y.; Han, J.; Zhang, Y., Growth of Cu2ZnSnSe4 Film under Controllable Se Vapor Composition and Impact of Low Cu Content on Solar Cell Efficiency. *ACS applied materials & interfaces* **2016,** *8* (16), 10283-92.
5. ElAnzeery, H.; El Daif, O.; Buffière, M.; Oueslati, S.; Ben Messaoud, K.; Agten, D.; Brammertz, G.; Guindi, R.; Kniknie, B.; Meuris, M.; Poortmans, J., Refractive index extraction and thickness optimization of Cu2ZnSnSe4 thin film solar cells. *physica status solidi (a)* **2015,** *212* (9), 1984-1990.